ADVANCED MATERIALS
www.advmat.de

Highly Tunable Thiol-Ene Photoresins for Volumetric Additive Manufacturing

*Caitlyn C. Cook, Erika J. Fong, Johanna J. Schwartz, Dominique H. Porcincula, Allison C. Kaczmarek, James S. Oakdale, Bryan D. Moran, Kyle M. Champley, Charles M. Rackson, Archish Muralidharan, Robert R. McLeod, and Maxim Shusteff**

Volumetric additive manufacturing (VAM) forms complete 3D objects in a single photocuring operation without layering defects, enabling 3D printed polymer parts with mechanical properties similar to their bulk material counterparts. This study presents the first report of VAM-printed thiol-ene resins. With well-ordered molecular networks, thiol-ene chemistry accesses polymer materials with a wide range of mechanical properties, moving VAM beyond the limitations of commonly used acrylate formulations. Since free-radical thiol-ene polymerization is not inhibited by oxygen, the nonlinear threshold response required in VAM is introduced by incorporating 2,2,6,6-tetramethyl-1-piperidinyloxy (TEMPO) as a radical scavenger. Tuning of the reaction kinetics is accomplished by balancing inhibitor and initiator content. Coupling this with quantitative measurements of the absorbed volumetric optical dose allows control of polymer conversion and gelation during printing. Importantly, this work thereby establishes the first comprehensive framework for spatial–temporal control over volumetric energy distribution, demonstrating structures 3D printed in thiol-ene resin by means of tomographic volumetric VAM. Mechanical characterization of this thiol-ene system, with varied ratios of isocyanurate and triethylene glycol monomers, reveals highly tunable mechanical response far more versatile than identical acrylate-based resins. This broadens the range of materials and properties available for VAM, taking another step toward high-performance printed polymers.

Volumetric additive manufacturing (VAM) is an emerging approach to photopolymer-based 3D printing that produces complex 3D structures in a single step, rather than from layer-by-layer assembly.[1] This paradigm holds promise because it overcomes many of the drawbacks of layer-based fabrication, such as long build times and rough surfaces. VAM also augurs a broadening of the materials available for photopolymer 3D printing, having fewer constraints on viscosity and reactivity compared to layerwise printing. Indeed, though VAM has been demonstrated with extremely soft hydrogels,[2,3] it has relied until now almost exclusively on acrylate-based chemistry.[4] This is natural, because the oxygen inhibition of acrylate polymerization provides the threshold behavior required for VAM. However, acrylate chemistry is in general limiting due to the brittle and glassy properties of the resulting materials. Accordingly, extensive efforts have been made to identify and target specific soft, elastic acrylate formulations.[5–9] Introducing alternative crosslinking chemistries to the VAM realm, as well as AM more broadly, is highly desirable as an alternative method to gain access to a wider range of mechanical, thermal, and optical performance.[10–14] Thiol-ene-based polymers are one class of materials that have drawn significant attention owing to their controllable, tunable mechanical properties.[15–17] This is generally attributed to more uniform molecular networks in thiol-ene materials, resulting from the step-growth mechanism of the polymerization reaction.[18,19] Thiol-ene materials have already shown promise for applications including use in adhesives, electronics, and as biomaterials.[20,21] This work expands the versatility of volumetric AM by introducing a new class of VAM-compatible thiol-ene resins. We demonstrate the formulation of thiol-ene resins with the nonlinear threshold-type kinetics required for VAM and show bulk-equivalent performance in the resulting 3D printed parts, confirming the advantage of the layerless whole-part process.

In our volumetric AM system, a 3D distribution of light energy is delivered to the resin vat by superimposing exposures from multiple angles, a method termed computed axial lithography (CAL) (**Figure 1**a).[2] The exposures are a sequence of projections calculated from 3D CAD models using algorithms from computed

C. C. Cook, Dr. E. J. Fong, Dr. J. J. Schwartz, D. H. Porcincula, A. C. Kaczmarek, Dr. J. S. Oakdale, B. D. Moran, Dr. K. M. Champley, Dr. M. Shusteff
Lawrence Livermore National Laboratory
Livermore, CA 94550, USA
E-mail: shusteff1@llnl.gov
C. M. Rackson, Prof. R. R. McLeod
Electrical, Computer, and Energy Engineering Department
University of Colorado
Boulder, CO 80309, USA
A. Muralidharan
Materials Science and Engineering Program
University of Colorado
Boulder, CO 80303, USA
The ORCID identification number(s) for the author(s) of this article can be found under https://doi.org/10.1002/adma.202003376.

DOI: 10.1002/adma.202003376

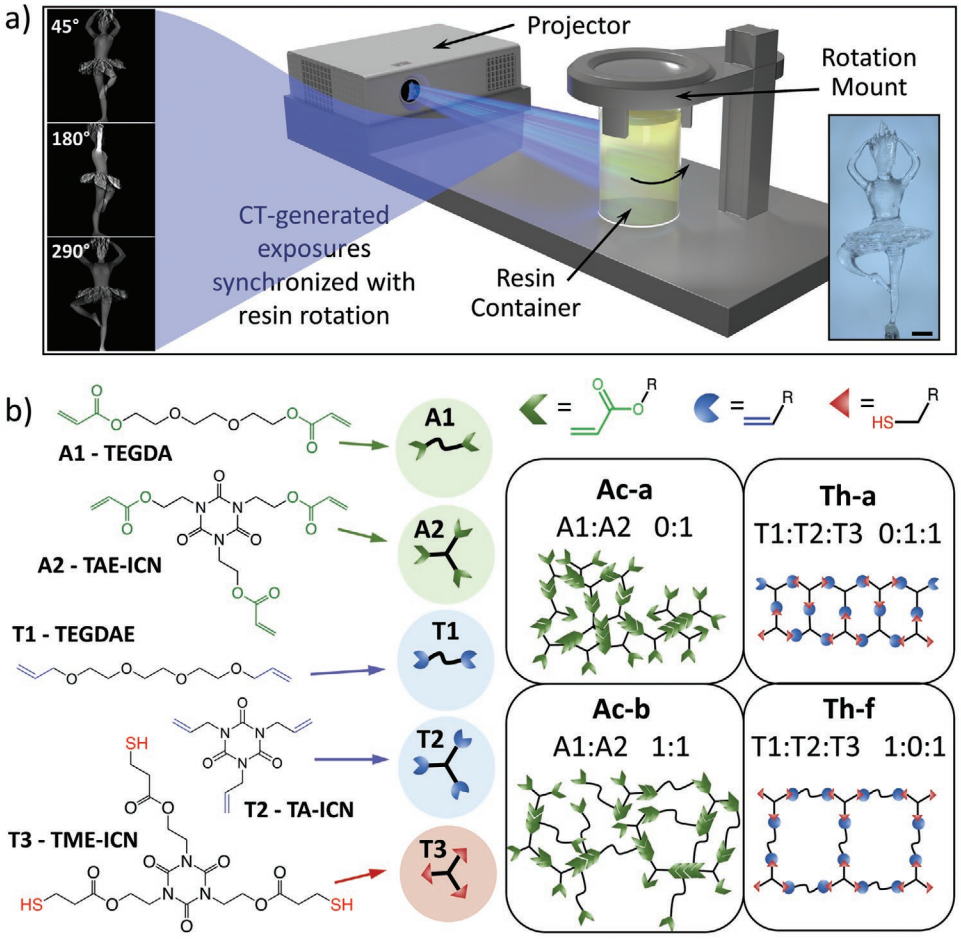

Figure 1. a) Schematic of VAM hardware configuration. The insets at left present example projections from different angles, resulting in the structure shown in the right inset. Scale bar: 2 mm. b) Schematics of four formulations Ac-a, Ac-b, Th-a, and Th-f, with varying molecular network structure composed of five constituent monomers, with acrylate (green) and thiol-ene (red/blue) functionality. Compositions are indicated by molar ratios of functional groups. A1—Triethylene glycol diacrylate (TEGDA), A2—Tris[2-(acryloyloxy)ethyl] isocyanurate (TAE-ICN), T1—Triethylene glycol diallyl ether (TEGDAE), T2—Tri-allyl isocyanurate (TA-ICN), and T3—Tris[2-(3-mercaptopropionyloxy)ethyl] isocyanurate (TME-ICN). The 3D model of the ballerina in Figure 1a by Miguel Zavala is licensed under the CC BY Creative Commons Attribution 4.0 International license (https://creativecommons.org/licenses/by/4.0).

tomography (CT). Resins used in VAM must have a nonlinear response to the curing illumination, with an energy threshold below which no significant polymerization takes place. This allows regions of the build volume that do not cross this threshold to remain liquid, and to be poured away after exposure. Resins that crosslink via acrylate functional groups naturally exhibit this nonlinear response as a consequence of the initial inhibition of the polymerization reaction by dissolved molecular oxygen.

In contrast, oxygen inhibition in radical initiated thiol-ene reactions is negligible, so our approach is to incorporate the nitroxide-based radical scavenger 2,2,6,6-tetramethyl-1-piperidinyloxy (TEMPO). TEMPO has proven to be a potent inhibitor of radical-mediated reactions[22,23] and was found in this work to be suitable for creating the nonlinear threshold behavior required for VAM. Other stabilizing agents were screened for possible use as inhibitors, but only TEMPO showed the needed threshold behavior (Figure S1, Supporting Information).

To exploit controlled thiol-ene network formation in VAM, we investigated thiol-ene and acrylate resin formulations differing only in their crosslinking chemistry. Four resins were formulated as shown in Figure 1b from five monomers, each containing either rigid (an isocyanurate ring (ICN)), or flexible (a triethylene glycol chain (TEG)) subunits for tunable mechanical response. The two thiol-ene resins paired a trithiol ICN monomer (T3) with either a triallyl ICN (T2) or a diallyl TEG (T1), referred to as Th-a and Th-f, respectively. We expected these to differ significantly in their molecular-scale network structure and connectivity. The two corresponding acrylate resins, referred to as Ac-a and Ac-b, respectively, were the triacrylate ICN (A2) on its own, or mixed 1:1 (moles of functional groups) with the diacrylate TEG (A1). Irgacure 907 (I907) was used as the photoinitiator (PI) in all formulations, due to its low-absorbance tail around the 405 nm spectral region relevant for our VAM system. In contrast to PI selection for layer-based printing, PIs for VAM should have a low molar extinction coefficient ε at the operating wavelengths, which allows for a sufficiently high concentration of PI while maintaining a large penetration depth. All resins used in this work were mixed with PI as the dominant absorbing species.

Figure 2a summarizes adjustment of the induction period in thiol-ene by the addition of TEMPO, measured using real-time

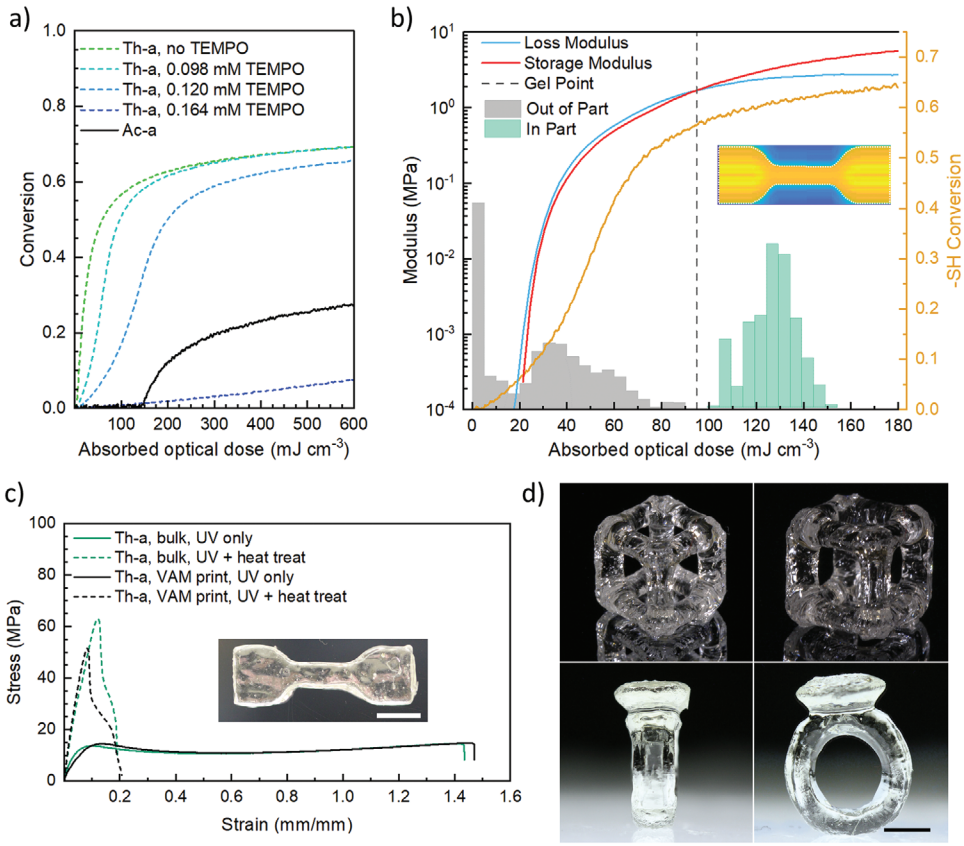

Figure 2. Adjustment of thiol-ene resin kinetics for VAM printing. a) Real-time FTIR data of thiol group conversion during Th-a resin polymerization (dashed lines, 40×10^{-3} M I907), showing an induction period tunable by varying TEMPO concentration, compared to the corresponding acrylate formulation Ac-a (solid line). b) Th-a formulation (10×10^{-3} M I907) photorheology and thiol conversion, overlaid with a histogram of the predicted doses in the build volume for a dog bone print. c) VAM printed and UV postcured dog bone samples show comparable tensile properties to bulk samples exposed to a similar absorbed optical dose, with properties remaining comparable after heat treatment. d) A complex cube and ring structure printed in Th-a resin using VAM. Scale bars: 5 mm.

Fourier transform infrared (FTIR) spectroscopy. Although the transition out of the induction period is not as sharp as in the corresponding acrylate, it is sufficient to enable controlled volumetric part formation. This is in large measure owing to much later gelation in the step-growth thiol-ene polymerization, compared with chain-growth propagation in acrylates.[19] Indeed, quantifying the absorbed optical energy needed to reach gelation is an essential control parameter for the VAM print process. This is referred to as the critical dose D_c (mJ cm^{-3}). The equivalent concept in layered stereolithography is known as the critical curing energy E_c, measured on an area basis (mJ cm^{-2}), and D_c is its volumetric counterpart. Although specifying a single value for D_c implies exposure reciprocity between intensity and duration, this is known to be inaccurate in a variety of situations.[24–26] At a minimum, the dose rate (dependent on the illumination intensity and resin's absorption coefficient) plays an important role in determining a resin's degree of cure. Figures S2b and S3 in the Supporting Information provide an example of dose rate dependent variation in thiol-ene conversion kinetics. For this reason, ex situ experiments to measure D_c and cure kinetics leading to gelation are carried out with illumination intensities matching the intensity range projected during VAM builds (5–10 mW cm^{-2}).

Experimental measurements of D_c are obtained from observing the resin curing by oscillatory photorheology (Figure 2b). Gelation occurs where the storage modulus exceeds the loss modulus. Here, as well as for FTIR measurements, we estimate the optical energy dose absorbed by the resin as $E_{abs} = I_0 \alpha e^{-\alpha z} t_e$, where I_0 is the irradiance at the surface (mW cm^{-2}), t_e is the exposure time, z is the depth into the sample, and $\alpha = 2.3 \varepsilon c_{PI}$ is the resin's absorption coefficient (incorporating the PI concentration c_{PI}, and its molar extinction coefficient ε). For generality, we refer readers to Figures S4 and S5 in the Supporting Information for a discussion of wavelength dependence in such calculations. The Th-a formulation with 0.1×10^{-3} M TEMPO and 10×10^{-3} M I907 is found to gel at a dose of 95 mJ cm^{-3}, at a thiol group conversion of ≈56% (Figure 2b), in contrast to 15–25% double bond conversion at gelation characteristic of multifunctional acrylates.[26–28]

These two properties of the resin, D_c and α, are the key input parameters for the CT algorithm along with the target geometry. The algorithm calculates the set of projected light intensity fields from all angles and estimates the volumetric optical dose distribution throughout the build volume. The overall approach for generating the set of projections is derived from previous work[2] (with modifications fully described in the Supporting

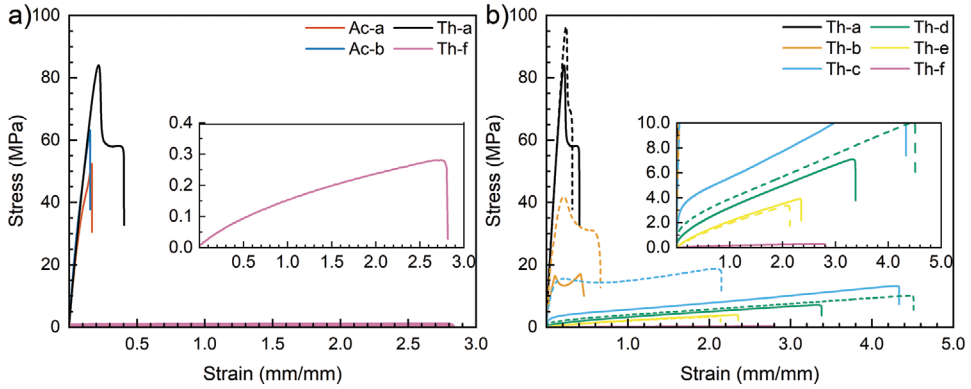

Figure 3. Tunable mechanical behavior of thiol-ene chemistry. a) Tensile response of thiol-enes Th-a and Th-f compared with acrylates Ac-a and Ac-b, composed of the same monomers and functionalities. b) Screening the full range of thiol-ene compositions presents a broad range of mechanical properties. Solid lines show the response of samples after light exposure only, and dashed lines show the same samples after thermal treatment (Note: the absorbed optical dose before heat treatment is much larger than for samples in Figure 2c).

Information). Briefly, rather than filtering the backprojections and imposing a positivity constraint,[3,4] we generate an initial estimate of the light intensity fields by using the (unfiltered) adjoint of the attenuated radon transform, weighted by using the simultaneous algebraic reconstruction technique (SART) algorithm applied in the reverse direction.[29] To obtain properly scaled physical units, the light intensity field calculation takes into account the resin's measured α, and is scaled by the desired critical dose D_c, and the estimated exposure time t_e, producing a quantitative prediction of the optical dose absorbed by every voxel in the build volume. Figure 2b overlays this predicted dose distribution (for the dogbone sample shown in the inset) on the resin curing data. The voxel histogram is subdivided into two populations: "in part" voxels (green) inside the target geometry that should receive a dose exceeding D_c, and "out of part" voxels (gray), which are outside of the geometry and should remain below the dose threshold. The initial estimate of the projected light intensity fields is iteratively optimized to maximize the separation between the "in part" and "out of part" groups. In practice, actual exposure time during a VAM build may vary slightly from the algorithmically predicted t_e, and changes in refractive index are used to visually detect part formation (Figures S6 and S7, Supporting Information). The actual dose delivered to the build volume is fine-tuned by adjusting the exposure time. Th-a dogbones were printed with exposures equivalent to D_c of 87–105 mJ cm^{-3}. By comparison, the acrylate resins require 300 mJ cm^{-3} for the best printing results. Similar CT-predicted dose distributions were calculated for more complex geometries, enabling the VAM printing of structures such as the cube and ring shown in Figure 2d.

One of the major benefits of VAM derives from layerless whole part printing, expected to produce uniform and isotropic materials superior to those from layer-by-layer 3D printing.[30,31] Evidence to support this expectation comes from mechanical characterization of the constituent materials and the resulting structures. Bulk tensile samples were prepared from Th-a resin, and exposed to a similar volumetric dose of 405 nm light to compare mechanical properties to VAM printed parts (Figure 2c). Tensile testing results indicate that the VAM printed and bulk cast dogbones have near-equivalent stress–strain profiles directly after exposure as well as after thermal postprocessing.

Mechanical testing of bulk samples revealed that samples derived from Th-a and Th-f resins showed a very wide range of mechanical performance, from stiff and tough to soft and rubbery (**Figure 3**a). Elastic moduli after UV exposure spanned three orders of magnitude (421 and 0.12 MPa), with failure strains of 44% and 293% for Th-a and Th-f samples, respectively. In contrast, the Ac-a and Ac-b formulations showed no such tunability: in spite of rather different monomer composition, both Ac-a and Ac-b yielded stiff and brittle polymers. To add to these observations, we screened thiol-ene compositions covering the full range of variation in mechanical properties from Th-a to Th-f. These are identified as Th-b to Th-e to indicate intermediate ratios of flexible diallyl PEG and rigid triallyl ICN monomers, while keeping total thiol and allyl groups in stoichiometric balance (Table S2 in the Supporting Information provides complete details). Bulk-cured samples of these formulations produced widely variable stress–strain behavior (Figure 3b). Additionally, postexposure thermal treatment had little impact on the mechanical properties of Ac-a and Ac-b, but dramatically changed mechanical properties of thiol-ene samples (Figure 3b; Figure S8, Supporting Information).

Dynamic mechanical thermal analysis (Figure S9, Supporting Information) showed the expected sharp and tunable glass transitions for thiol-ene samples compared to the broad transitions of acrylate samples. This confirmed our expectations of more homogeneous, uniform molecular networks in thiol-enes that result in controlled mechanical properties. We also observed the increased toughness enabled by thiol-ene chemistry: although both Ac-a and Th-a have similar moduli and are based on similar trifunctional monomers, Th-a is 1.6 times tougher and has a 2.2 times higher elongation to break. Among the intermediate compositions, Th-c reaches a maximum toughness of 36 MJ m^{-3}.

The widely adjustable and bulk-equivalent mechanical behavior of this thiol-ene resin system represents a significant advancement for VAM, introducing a major class of polymer materials for use with the volumetric 3D printing paradigm. By varying the relative monomer composition within thiol-ene resins, the modulus and toughness can be varied by over two orders of magnitude, from 0.12 to 421 MPa, and 0.50 to 36 mJ m^{-3}, respectively, and the ultimate strain over one order of magnitude, from 36.1% to 293%. Since acrylate resins lack

this versatility, adapting thiol-enes for use in VAM presents an appealing avenue for further 3D printed polymer development, toward the ultimate goal of high-performance printed engineering polymers. We are particularly interested in utilizing these thiol-ene materials downstream as functional biological scaffolds, as the unreacted thiols can be used for downstream surface functionalization.[32–34] Providing threshold functionality by means of the radical-trapping inhibitor TEMPO points toward a general approach for formulating VAM-compatible materials, whether oxygen-inhibited or not. The sharpness of the threshold and its interplay with printing resolution and part mechanical properties warrant further investigation. More broadly, this work delineates a complete framework for quantitatively measuring and controlling the spatial–temporal optical energy dose distribution in VAM. Matching ex situ measurements of absorbed optical dose, with dose delivered in a VAM build creates a common reference scale for controlled 3D fabrication, and for useful comparisons among resin systems. Continued improvement of the quantitative agreement between algorithmic absorbed optical energy estimates, and experimental exposures will come from finer characterization of resin curing kinetics at varying dose rates, and incorporation of the photochemical behavior into the CT computational framework. As material choices continue to expand, advancements like this pave the way for further research into spatial–temporal control of polymerization in complex resin systems.

Experimental Section

Materials: Poly(ethylene glycol) diacrylate (Mn 250) (TEG-DA), Tris[2-(acryloyloxy)ethyl] isocyanurate (TAE-ICN), 1,3,5-triallyl-1,3,5-triazine-2,4,6(1*H*,3*H*,5*H*)-trione (TA-ICN), 2-methyl-4′-(methylthio)-2-morpholinopropiophenone or Irgacure 907, and TEMPO were purchased from Sigma-Aldrich, and Tris[2-(3-mercaptopropionyloxy) ethyl] isocyanurate (TME-ICN) was purchased from TCI America. All chemicals were used without further purification. Triethylene glycol diallyl ether (TEG-DAE) was synthesized following previously published procedures.[35,36]

Sample Preparation: Bulk samples for mechanical testing (Figure 3; Figures S4 and S5 and Tables S2 and S3, Supporting Information) were prepared as stoichiometric mixtures with 40×10^{-3} M I907, and exposed to a 405 nm LED flood cure (UV Curing Chamber, XYZprinting) at 18 mW cm^{-2} for 20 min (E_{abs} estimate 20 000 mJ cm^{-3}). These samples were heat treated for 1 h at 190 °C and 15 h at 120 °C, for acrylates and thiol-enes, respectively. Heat treatment is a well-established means to improve conversion, and thereby mechanical properties, of UV-cured acrylate and thiol-ene parts.[37] For VAM printing, Th-a resin was formulated with 0.1×10^{-3} M TEMPO and 10×10^{-3} M I907, and postcured after printing with 405 nm light at 2 mW cm^{-2} for 20 min (Helix Cure 60, Strategic 3D Solutions - E_{abs} estimate 450 mJ cm^{-3}). Bulk samples of Th-a resin for direct comparison with VAM prints (Figure 2c) were exposed with a mercury arc lamp (Omnicure S2000, Excelitas) through a narrow-band 405nm filter (FBH405-10, Thorlabs) for 20 min at 18 mW cm^{-2} (E_{abs} estimate 1100 mJ cm^{-3}). The absorbed optical energy of these samples (a well as the VAM prints) was significantly lower than for the bulk samples of Figure 3, and for this reason heat treatment (120 °C for 15 h) had more pronounced effect on the modulus and elongation of these samples. The same arc lamp and 405 nm filter were used for illumination during real-time FTIR and photorheology measurements, with intensity adjusted to 5 and 7 mW cm^{-2}, respectively.

Volumetric Printing Procedure: VAM prints were performed in a custom printer setup equipped with a 405 nm LED light engine (CEL5500, Digital Light Innovations), with a maximum intensity of 55 mW cm^{-2}, illuminating a resin vial fixtured to a rotation mount (HDR50, ThorLabs). Output of all light sources was measured using a Si photodiode power meter, and spectral distribution measured using a compact CCD spectrometer (PM100D with S120VC sensor, and CCS100, Thorlabs). Spectral information for all light sources is given in the Supporting Information, along with methods for calculating wavelength-dependent absorbed optical dose in each case.

Additional characterization methods, tomographic modeling, and volumetric projection can be found in the Supporting Information.

Supporting Information

Supporting Information is available from the Wiley Online Library or from the author.

Acknowledgements

The authors gratefully acknowledge Taylor Bryson for carrying out DMA measurements and April Sawvel and the Center for National Security Applications of Magnetic Resonance for help with solid-state NMR. This work was performed under the auspices of the U.S. Department of Energy by Lawrence Livermore National Laboratory under Contract DE-AC52-07NA27344. Funding provided by the LLNL LDRD Program LLNL-JRNL-809451.

Conflict of Interest

The authors declare no conflict of interest.

Keywords

acrylate, photopolymerization, thiol-ene, tomography, volumetric additive manufacturing

Received: May 17, 2020
Revised: July 20, 2020
Published online:

[1] M. Shusteff, A. E. M. Browar, B. E. Kelly, J. Henriksson, T. H. Weisgraber, R. M. Panas, N. X. Fang, C. M. Spadaccini, *Sci. Adv.* **2017**, *3*, eaao5496.
[2] B. E. Kelly, I. Bhattacharya, H. Heidari, M. Shusteff, C. M. Spadaccini, H. K. Taylor, *Science* **2019**, *363*, 1075.
[3] P. N. Bernal, P. Delrot, D. Loterie, Y. Li, J. Malda, C. Moser, R. Levato, *Adv. Mater.* **2019**, *31*, 1904209.
[4] D. Loterie, P. Delrot, C. Moser, *Nat. Commun.* **2020**, *11*, 852.
[5] L. Zhou, J. Fu, Y. He, *Adv. Funct. Mater.* **2020**, *30*, 2000187.
[6] S. Clark Ligon-Auer, M. Schwentenwein, C. Gorsche, J. Stampfl, R. Liska, *Polym. Chem.* **2016**, *7*, 257.
[7] D. K. Patel, A. H. Sakhaei, M. Layani, B. Zhang, Q. Ge, S. Magdassi, *Adv. Mater.* **2017**, *29*, 1606000.
[8] C. J. Thrasher, J. J. Schwartz, A. J. Boydston, *ACS Appl. Mater. Interfaces* **2017**, *9*, 39708.
[9] Y. Deng, J. Li, Z. He, J. Hong, J. Bao, *J. Appl. Polym. Sci.* **2020**, *137*, 49294.
[10] M. D. Alim, K. K. Childress, N. J. Baugh, A. M. Martinez, A. Davenport, B. D. Fairbanks, M. K. McBride, B. T. Worrell, J. W. Stansbury, R. R. McLeod, C. N. Bowman, *Mater. Horiz.* **2020**, *7*, 835.

[11] K. L. Wiley, E. M. Ovadia, C. J. Calo, R. E. Huber, A. M. Kloxin, *Polym. Chem.* **2019**, *10*, 4428.
[12] K. K. Childress, M. D. Alim, J. J. Hernandez, J. W. Stansbury, C. N. Bowman, *Polym. Chem.* **2020**, *11*, 39.
[13] D. G. Sycks, T. Wu, H. S. Park, K. Gall, *J. Appl. Polym. Sci.* **2018**, *135*, 46259.
[14] J. Zhou, Q. Zhang, S. Chen, H. Zhang, A. Ma, M. Ma, Q. Liu, J. Tan, *Polym. Test.* **2013**, *32*, 608.
[15] M. Sahin, S. Ayalur-Karunakaran, J. Manhart, M. Wolfahrt, W. Kern, S. Schlögl, *Adv. Eng. Mater.* **2017**, *19*, 1600620.
[16] H. B. Song, A. Baranek, B. T. Worrell, W. D. Cook, C. N. Bowman, *Adv. Funct. Mater.* **2018**, *28*, 1801095.
[17] T. J. McKenzie, P. S. Heaton, K. Rishi, R. Kumar, T. Brunet, G. Beaucage, O. Mondain-Monval, N. Ayres, *Macromolecules* **2020**, *53*, 3719.
[18] C. E. Hoyle, T. Y. Lee, T. Roper, *J. Polym. Sci., Part A: Polym. Chem.* **2004**, *42*, 5301.
[19] C. E. Hoyle, C. N. Bowman, *Angew. Chem., Int. Ed.* **2010**, *49*, 1540.
[20] P. M. Kharkar, M. S. Rehmann, K. M. Skeens, E. Maverakis, A. M. Kloxin, *ACS Biomater. Sci. Eng.* **2016**, *2*, 165.
[21] T. O. Machado, C. Sayer, P. H. H. Araujo, *Eur. Polym. J.* **2017**, *86*, 200.
[22] S. Chatani, T. Gong, B. A. Earle, M. Podgórski, C. N. Bowman, *ACS Macro Lett.* **2014**, *3*, 315.
[23] P. J. Wright, A. M. English, *J. Am. Chem. Soc.* **2003**, *125*, 8655.
[24] L. Feng, B. I. Suh, *Macromol. Chem. Phys.* **2007**, *208*, 295.
[25] J. W. Wydra, N. B. Cramer, J. W. Stansbury, C. N. Bowman, *Dent. Mater.* **2014**, *30*, 605.
[26] A. C. Uzcategui, A. Muralidharan, V. L. Ferguson, S. J. Bryant, R. R. McLeod, *Adv. Eng. Mater.* **2018**, *20*, 1800876.
[27] C. Gorsche, R. Harikrishna, S. Baudis, P. Knaack, B. Husar, J. Laeuger, H. Hoffmann, R. Liska, *Anal. Chem.* **2017**, *89*, 4958.
[28] A. Muralidharan, A. C. Uzcategui, R. R. McLeod, S. J. Bryant, *Adv. Mater. Technol.* **2019**, *4*, 1900592.
[29] A. Andersen, *Ultrason. Imaging* **1984**, *6*, 81.
[30] S. C. Ligon, R. Liska, J. Stampfl, M. Gurr, R. Mülhaupt, *Chem. Rev.* **2017**, *117*, 10212.
[31] M. Monzón, Z. Ortega, A. Hernández, R. Paz, F. Ortega, *Materials* **2017**, *10*, 64.
[32] S. Caldwell, D. W. Johnson, M. P. Didsbury, B. A. Murray, J. J. Wu, S. A. Przyborski, N. R. Cameron, *Soft Matter* **2012**, *8*, 10344.
[33] J. D. Krutty, S. K. Schmitt, P. Gopalan, W. L. Murphy, *Curr. Opin. Biotechnol.* **2016**, *40*, 164.
[34] B. Grigoryan, S. J. Paulsen, D. C. Corbett, D. W. Sazer, C. L. Fortin, A. J. Zaita, P. T. Greenfield, N. J. Calafat, J. P. Gounley, A. H. Ta, F. Johansson, A. Randles, J. E. Rosenkrantz, J. D. Louis-Rosenberg, P. A. Galie, K. R. Stevens, J. S. Miller, *Science* **2019**, *364*, 458.
[35] J. V. Crivello, K. D. Jo, *J. Polym. Sci., Part A: Polym. Chem.* **1993**, *31*, 1473.
[36] A. Rusli, W. Cook, G. G. Liang, *Eur. Polym. J.* **2011**, *47*, 1785.
[37] J. Dai, S. Ma, L. Zhu, S. Wang, L. Yang, Z. Song, X. Liu, J. Zhu, *Polymer* **2017**, *108*, 215.